RSC Advances

PAPER

View Article Online
View Journal | View Issue

Cite this: *RSC Adv.*, 2024, **14**, 38222

Gas-phase aldol condensation of formaldehyde to produce hydroxyacetaldehyde and its implication to new particle formation: a theoretical study†

Nianchi Tang,‡[a] Lijuan Zhang,‡[a] Jiao Chen,[b] Yue Pan,[c] Hongyang Xu[a] and Chunyu Wang *[a]

Aldehydes have been proposed as important precursor species in new particle formation (NPF). Although formaldehyde (CH_2O) has minimal direct involvement in sulfuric acid (H_2SO_4) and water nucleation, it remains unclear whether its atmospheric aldol condensation product, hydroxyacetaldehyde ($C_2H_4O_2$), one of the simplest bifunctional oxygenated volatile organic compounds (OVOCs), plays a role in NPF. This study investigates both the aldol condensation of CH_2O and its role in NPF involving H_2SO_4 and $C_2H_4O_2$ through quantum chemical calculations and atmospheric cluster dynamics modeling. Kinetic calculations indicate that the reaction rate of CH_2O aldol condensation catalyzed by H_2SO_4 is 8 to 16 orders of magnitude higher than that of the uncatalyzed pathway at 200–298 K. Based on molecular structures and formation Gibbs free energies, interactions between sulfuric acid/its polymers and $C_2H_4O_2$ are thermodynamically favorable. Furthermore, $C_2H_4O_2$, with its hydroxyl group, stabilizes H_2SO_4 clusters more effectively than CH_2O, thereby enhancing nucleation. Additional cluster kinetic modeling suggests that particle formation rates in this system exceed those in the sulfuric acid–water binary system under conditions of low ambient H_2SO_4 concentrations and low relative humidity. However, cluster growth remains limited due to weak formation of larger clusters, indicating that other stabilizing vapors are needed for sustained cluster growth and stable particle formation.

Received 13th November 2024
Accepted 27th November 2024

DOI: 10.1039/d4ra08063g

rsc.li/rsc-advances

1. Introduction

The formation of atmospheric particles is of great interest because of the atmospheric particles' impact on global climate and health.[1–3] New particle formation (NPF) accounts for over 50% of atmospheric cloud condensation nuclei (CCN), significantly impacting cloud properties and Earth's energy balance.[4] Despite this importance, the chemical identity and relative significance of participating vapors remain insufficiently understood. Sulfuric acid (H_2SO_4) is widely recognized as a critical nucleation precursor in the atmosphere due to its extremely low volatility and high acidity.[5,6] However, both sulfuric acid–water (H_2SO_4–H_2O) binary nucleation and ternary nucleation involving ammonia or amines fail to fully explain observed NPF events under the complex and varied conditions of the atmosphere,[7–12] indicating other chemical species may also play important roles in NPF.[6,13,14]

Formaldehyde (CH_2O) is a compound of significant interest due to its critical role as an intermediate in atmospheric photochemical reactions, where it notably enhances both atmospheric reactivity and oxidative capacity. Furthermore, given its wide range of applications, exposure to CH_2O is linked to both acute and chronic health effects.[15] Its atmospheric concentrations vary widely, ranging from several thousand pptv to tens of ppbv, depending on geographic and environmental factors.[16–18] Budget analyses of CH_2O show significant discrepancies between observed concentrations and those predicted by models.[19,20] This has prompted increased interest in alternative CH_2O removal mechanisms, including uptake by soil surfaces,[21] aerosols/clouds,[22–24] as well as its direct participation in nucleation processes.[25–27] These pathways may represent additional sinks for CH_2O, offering potential explanations for the overestimation of its concentrations in atmospheric models. Our previous flow tube experiments indicate that the enhancement of CH_2O in H_2SO_4–H_2O homogeneous nucleation is negligible.[26] However, we also discovered that the hydrolysis product of CH_2O, methanediol ($CH_2(OH)_2$), forms hydrogen bonds with sulfuric acid and its polymer through its hydroxyl groups, thereby contributing to cluster stabilization.[28] The possible

[a]*School of Biological and Environmental Engineering, Chaohu University, Chaohu Regional Collaborative Technology Service Center for Rural Revitalization, Hefei, Anhui 238000, China. E-mail: cyw2022@chu.edu.cn*

[b]*Anhui Meteorological Observatory, Hefei, Anhui 230031, China*

[c]*School of Electronic Engineering, Chaohu University, Hefei, Anhui 238000, China*

† Electronic supplementary information (ESI) available: Cluster formation energies from monomers for $(H_2SO_4)_m(C_2H_4O_2)_n$ ($0 \le m$, $n \le 3$) and all Cartesian coordinates of optimized global Gibbs free energy minima for $(SA)_m(C_2H_4O_2)_n$ ($0 \le m$, $n \le 3$), $(H_2SO_4)_m(NH_3)$ ($0 \le m \le 3$), and $(H_2SO_4)_m(H_2O)$ ($0 \le m \le 3$). See DOI: https://doi.org/10.1039/d4ra08063g

‡ These authors contributed equally to this work.

product of atmospheric formaldehyde *via* aldol condensation is hydroxyacetaldehyde (glycolaldehyde, $C_2H_4O_2$).[29] Despite this, the kinetics of CH_2O aldol condensation remain insufficiently understood, and its potential involvement in NPF is unknown. Previous studies have demonstrated that the products of aldehyde aldol condensation can contribute to particle growth in the atmosphere.[25,30,31] For instance, Shi *et al.*[25] found that atmospheric aldol condensation products of aldehydes are more likely to form clusters with sulfuric acid than the aldehydes themselves, as demonstrated by quantum chemical calculations. Therefore, it is systematic and meaningful to further investigate the impact of $C_2H_4O_2$ on NPF.

As one of the simplest bifunctional oxygenated volatile organic compounds (OVOCs), $C_2H_4O_2$ contains both aldehyde and alcohol functional groups. It is primarily produced from isoprene[32] (468 Tg C per year, with 22% gas phase conversion to $C_2H_4O_2$ *via* hydroxyl radicals[33]) and ethene,[34] and has been detected in biomass burning plumes.[35] Its ambient concentration is approximately one-seventh that of formaldehyde,[36] indicating that the concentration of $C_2H_4O_2$ ranges from hundreds of pptv to several ppbv in various regions of the world. In the Southeastern U.S.A., measurements over a forested areas below 2 km altitude have recorded levels of up to 3 ppbv, with a mean concentration of 1 ppbv.[37] In addition to structural hydroxyl content and high concentration, indicating the possible involvement in NPF, $C_2H_4O_2$ also exhibits a relatively low vapor pressure. Estimated at 8.32×10^5 atm at 298 K, this vapor pressure is notably lower than that of CH_2O (*i.e.* 5.13 atm).[29] Due to this reduced volatility, $C_2H_4O_2$ molecules are more prone to condensation, thereby contributing to atmospheric particle growth. Bulk aqueous hydroxyl radicals with $C_2H_4O_2$ experiments performed by Perri *et al.*[38] show that $C_2H_4O_2$ (as well as glyoxal and methylglyoxal) is an important source of secondary organic aerosol. Recent research indicates that the decomposition of $C_2H_4O_2$ could represent a significant initial step in new particle formation, based on thermodynamic calculations.[39] Nevertheless, further kinetics investigation including collision and evaporation rate is required to delineate the mechanism of new particle formation.

In this study, we investigate the catalytic effect of sulfuric acid (SA) in the aldol condensation of CH_2O to produce $C_2H_4O_2$ and conduct a comparative analysis of molecular cluster formation between SA and CH_2O, as well as SA and $C_2H_4O_2$, using a combination of quantum chemical calculations and kinetic modeling *via* the Atmospheric Cluster Dynamics Code (ACDC).[40,41] After performing systematic conformational searches, we obtained minimum Gibbs free energy structures of clusters with compositions $(SA)_m(B)_n$ ($0 \le m, n \le 3$; "B" represents CH_2O or $C_2H_4O_2$). The corresponding thermodynamic data were then applied in ACDC to obtain particle formation rates. Furthermore, the effect of the vapor concentrations on cluster formation was assessed.

2. Methods

2.1. Quantum chemical calculations

The basin-hopping (BH) algorithm[42–44] coupled with the PM7 semiempirical potential[45] implemented in the MOPAC 2016 program (**https://openmopac.net**) was employed to search for the initial $(SA)_m(B)_n$ ($0 \le m, n \le 3$; "B" represents CH_2O or $C_2H_4O_2$) geometries, which is similar to our previous studies.[28,46–48] Then, the top 20 lowest-lying conformers of each clusters were optimized at the PW91PW91/6-311++G(3df,3pd) level to determine the final configurations with the Gaussian 09 software package.[49] Harmonic vibrational frequencies were calculated to confirm that these obtained conformers were the true minima. The method provides good geometries,[50,51] excellent vibrational frequencies[52] and quite accurate cluster Gibbs free energies compared with the currently available experiments.[53–55] Benchmark details of the methods employed in atmospheric cluster calculations can be found in our previous study.[26]

2.2. Kinetics calculations

For kinetic calculations, geometry optimization of all reactants, prereaction complexes, transition states, postreaction complexes, and products were performed using M06-2X[56] functional at the 6-311++G(d,p)[57] basis set with the Gaussian 09 software package. Furthermore, intrinsic reaction coordinate (IRC) calculations[58] were performed at the same level to determine whether the located transition states connect with the desired reactants and products. In addition, to refine the relative energies of the various stationary points, single-point energy calculations were carried out at the DLPNO-CCSD(T)/aug-cc-pVTZ level of theory with the ORCA 4.0 suite of programs.[59] To evaluate the effects of SA on the rate constants of the gas-phase aldol condensation of CH_2O, conventional transition-state theory (TST) with Eckart tunneling correction[60,61] was used to calculated reaction rate constants with the KiSThelP program.[62]

We used the ACDC to study formation rates and evaporation properties of $(SA)_m(B)_n$ ($0 \le m, n \le 3$; "B" represents CH_2O or $C_2H_4O_2$) clusters. The code generates and solves the cluster birth-death equations, the time derivatives of the concentrations of all constituents included in the simulation, which essentially is a series of logical checks over all possible cluster combinations to see which evaporations and collisions can create or destroy a given cluster.[41,63,64] The code generates and solves the cluster birth-death equations, the time derivatives of the concentrations of all constituents included in the simulation as eqn (1):

$$\frac{dc_i}{dt} = \frac{1}{2}\sum_{j<i}\beta_{j,(i-j)}c_j c_{(i-j)} + \sum_j \gamma_{(i+j)\to i}c_{i+j} - \sum_j \beta_{i,j}c_i c_j - \frac{1}{2}\sum_{j<i}\gamma_{i\to j}c_i + Q_i - S_i \quad (1)$$

where c_i is the concentration of cluster i, $\beta_{i,j}$ is the collision coeffcient of clusters i with j, and $\gamma_{i+j\to j}$ is the evaporation coeffcient of cluster $i + j$ evaporating into clusters i and j. Q_i is the possible additional source of cluster i and S_i is the sink term of cluster i. The collision rate constants were calculated from the kinetic gas theory, and the evaporation rate constants were calculated from the Gibbs free energies of formation of the clusters according to the concept of detailed balance.

$$\gamma_{(i+j)\rightarrow i} = \beta_{ij}\frac{c_i^e c_j^e}{c_{i+j}^e} = \beta_{ij} c_{\mathrm{ref}} \exp\left(\frac{\Delta G_{i+j} - \Delta G_i - \Delta G_j}{k_b T}\right) \quad (2)$$

where c_i^e is the equilibrium concentration of cluster i, ΔG_i is the Gibbs free energy of the formation of cluster i, and c_{ref} is the monomer concentration of the reference vapor corresponding to the pressure of 1 atm at which the Gibbs free energies were determined.

In addition, the cluster formation rate in our study is defined as the flux of clusters outside the "3 × 3 box" system, where 3 is the maximum number of H_2SO_4, CH_2O or $C_2H_4O_2$ in the clusters, assuming the clusters on the boundaries are large enough to have negligible evaporation coefficients, since these clusters are not allowed to re-enter, it is as if they have become stable particles. A constant coagulation sink coefficient (sink term) and the source rate was set to zero for simplicity.

3. Results and discussion

3.1. Aldol condensation of formaldehyde without/with catalyzed sulfuric acid

Given the estimated standard formation Gibbs free energy (ΔG_f^0) of CH_2O and β-hydroxycarbonyl, $C_2H_4O_2$, summarized by Barsanti and Pankow (−102.5 and −270.4 kJ mol^{-1}),[29] the standard Gibbs free energies changes (ΔG^0) for formaldehyde aldol condensation is −15.63 kcal mol^{-1} according to the fundamental eqn (3), indicating the reaction is favorable.

$$\Delta G^0 = \sum_i \nu_i \Delta G_{f,i}^0 \quad (3)$$

The formation of $C_2H_4O_2$ *via* aldol condensation can be expressed as

$$CH_2O + CH_2O \rightleftharpoons C_2H_4O_2 \quad (4)$$

There exist numerous reports on atmospherically proton transfer reactions and sulfuric acid can act as relatively strong hydrogen-atom donors/acceptors,[65–67] thereby possibly catalyzing the aldol condensation of CH_2O. In the presence of the catalyst H_2SO_4, they are trimolecular reaction systems, the reaction proceeds *via* collision with each other to form dimers, and then the dimers encounter the third reactant to form the $(CH_2O)_2(H_2SO_4)$ complex, which is followed by unimolecular transformation to form $(C_2H_4O_2)(H_2SO_4)$ complex in the exit channel. There are two possible entrance channels in the reaction of $CH_2O + CH_2O + H_2SO_4 \rightarrow C_2H_4O_2 + H_2SO_4$, and they can be expressed as

$$H_2SO_4 + CH_2O \rightleftharpoons (H_2SO_4)(CH_2O) \quad (5)$$

$$CH_2O + (H_2SO_4)(CH_2O) \rightarrow C_2H_4O_2 + H_2SO_4 \quad (6)$$

and

$$CH_2O + CH_2O \rightleftharpoons (CH_2O)_2 \quad (7)$$

$$(CH_2O)_2 + H_2SO_4 \rightarrow C_2H_4O_2 + H_2SO_4 \quad (8)$$

From the perspective of spatial structure, $(H_2SO_4)(CH_2O)$ reacts more readily, and the binding energy of the $(H_2SO_4)(CH_2O)$ (−10.6 kcal mol^{-1}) is lower than that of $(CH_2O)_2$ (−2.6 kcal mol^{-1}) as shown in Fig. 1. Therefore, the $(H_2SO_4)(CH_2O)$ + CH_2O entrance channel is considered here.

For the direct aldol condensation of CH_2O without a catalyst reaction (Fig. 1a), the fairly high reaction barrier resulting in the reaction is not a plausible path. The energy barrier is calculated to be 78.4 kcal mol^{-1} with respect to the prereactive complex and a large ring tension of the rather closed four-membered ring is in the transition state (TS1) geometry, making the path kinetically unfavorable. For the reaction catalyzed by H_2SO_4 (Fig. 1b), the energy barrier is calculated to be 39.2 kcal mol^{-1} with respect to the reactants CH_2O and $(H_2SO_4)(CH_2O)$, and it is clear that the reaction energy barrier of CH_2O aldol condensation catalyzed by H_2SO_4 is reduced by 39.2 kcal, which indicates

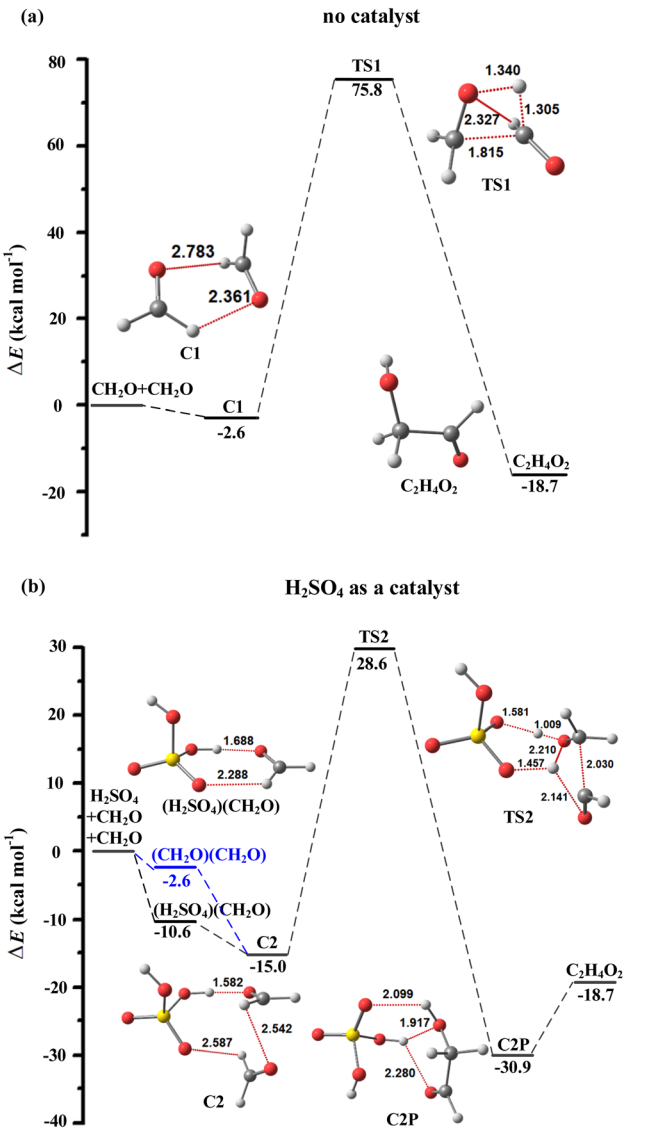

Fig. 1 Potential electronic energy surfaces with zero-point vibrational energies corrected at the DLPNO-CCSD(T)/aug-cc-pVTZ//M06-2X/6-311++G(d,p) level of theory (in kcal mol^{-1}) for the reaction of CH_2O + CH_2O with (a) no catalyst and (b) H_2SO_4 as a catalyst.

that the H_2SO_4 exerts a strong catalytic effect. However, the relatively high reaction barrier causes the reaction to be difficult to occur as well.

The atmospheric implications of the reactions studied would be determined by how fast different reaction channels are and the competition between them, so the reaction rate coefficients are calculated here. Applying the steady-state approximation to the prereactive complex and assuming that the complex is in equilibrium with the reactant, similar to the formation of H_2SO_4 (ref. 68) and organic nitrate,[69] the H_2SO_4-catalyzed formation reaction rate of $C_2H_4O_2$ ($v_{H_2SO_4}$) can be described as eqn (9):

$$v_{H_2SO_4} = \frac{d[C_2H_4O_2]}{dt} = K_{(H_2SO_4)(CH_2O)} \times k_4 \times [H_2SO_4][CH_2O]^2 \quad (9)$$

k_4 represents the bimolecular rate constants of the $(H_2SO_4)(CH_2O)$ + CH_2O reaction, which has been calculated using conventional transition-state theory with Eckart tunneling. The overall rate constant of the H_2SO_4-catalyzed formaldehyde aldol condensation ($k_{eff,\ H_2SO_4}$) is represented by eqn (8):

$$k_{eff,\ H_2SO_4} = K_{(H_2SO_4)(CH_2O)} \times k_4 \times [H_2SO_4] \quad (10)$$

The rate constants for each channel and equilibrium constants over the temperature range of 200–298 K are presented in Table 1. Without considering the catalyst, the rate constant k_{un} is 9.84×10^{-81} to 6.52×10^{-64} cm^3 per molecule per s at 200–298 K, which is too small for the reaction to occur. In the H_2SO_4 catalytic channel, the reaction rate constant is 2.23

Table 1 Equilibrium constants ($K_{(H_2SO_4)(CH_2O)}$, cm^3 per molecules), the reaction rate coefficients (k, cm^3 per molecule per s), and the reaction rates (v, molecules per cm^3 per s) for the formation of $C_2H_4O_2$ without/with catalyzed sulfuric acid between 200 and 298 K calculated at the DLPNO-CCSD(T)/aug-cc-pVTZ//M06-2X/6-311++G(d,p) level of theory

M	200 K	220 K	240 K	260 K	280 K	298 K
$K_{(H_2SO_4)(CH_2O)}$	2.31×10^{-15}	2.15×10^{-16}	3.01×10^{-17}	5.77×10^{-18}	1.42×10^{-18}	4.74×10^{-19}
k_6 [a]	9.65×10^{-57}	1.70×10^{-53}	1.34×10^{-50}	4.57×10^{-48}	7.44×10^{-46}	4.24×10^{-44}
k_{un} [b]	9.88×10^{-81}	3.94×10^{-76}	2.56×10^{-72}	5.20×10^{-69}	3.74×10^{-66}	6.55×10^{-64}
k_{eff} [c]	2.23×10^{-64}	3.65×10^{-62}	4.03×10^{-60}	2.64×10^{-58}	1.05×10^{-56}	2.01×10^{-55}
v_{eff}/v_{un} [d]	2.26×10^{16}	9.28×10^{13}	1.57×10^{12}	5.08×10^{10}	2.82×10^{9}	3.07×10^{8}

[a] The rate constant of the reaction of CH_2O + $(H_2SO_4)(CH_2O)$. [b] The rate constant of the reaction of CH_2O + CH_2O. [c] $[H_2SO_4]$ is 10^7 molecules per cm^3. [d] The relative rate ratio between CH_2O + CH_2O + H_2SO_4 and CH_2O + CH_2O when $[H_2SO_4]$ is 10^7 molecules per cm^3.

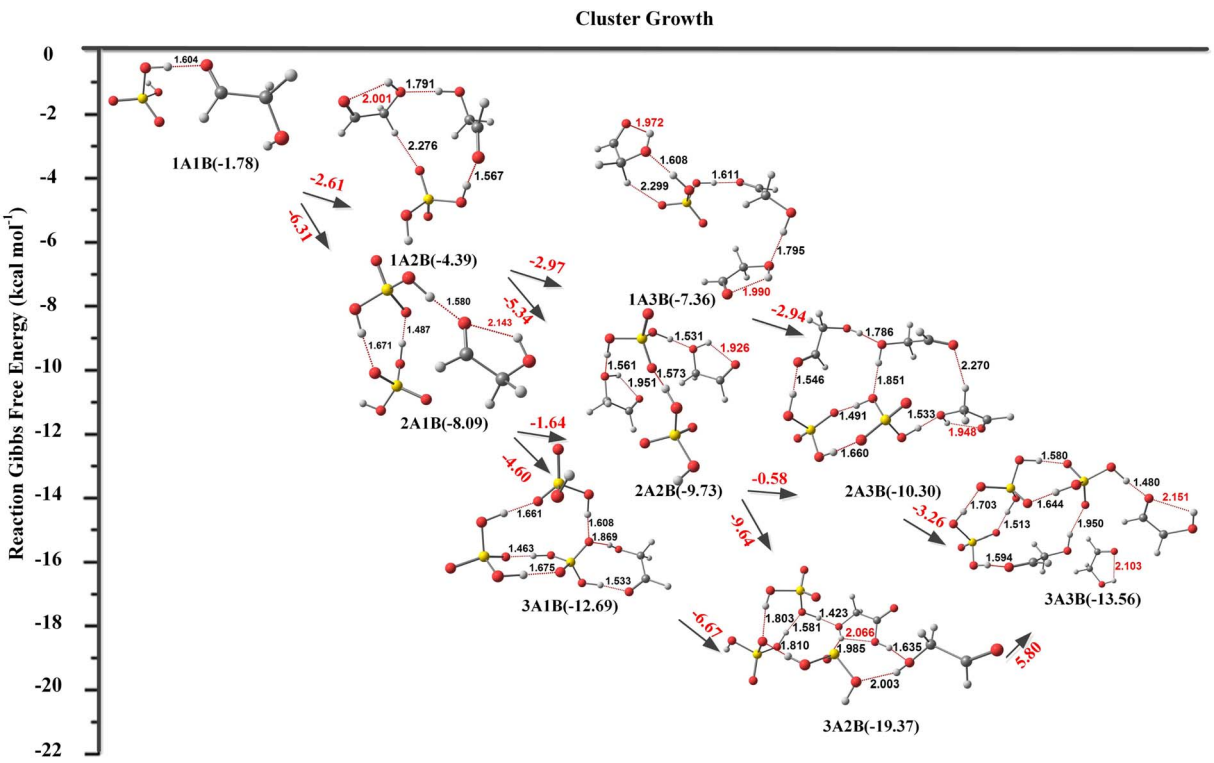

Fig. 2 Diagram for the studied cluster formation steps, with structures of global Gibbs free energy minima in the $(H_2SO_4)_m(C_2H_4O_2)_n$ ($m = 1–3$, $n = 1–3$) system obtained at the PW91PW91/6-311++G(3df,3pd) level of theory. All presented values are the calculated Gibbs free energy changes and the values in parentheses are the binding Gibbs free energies in kcal mol^{-1} at 298.15 K and 1 atm.

$\times 10^{-64}$ to 2.01×10^{-55} cm^3 per molecule per s at a typical atmospheric $[H_2SO_4]$ of 10^7 molecules per cm^3, where the H_2SO_4 concentrations in the atmosphere span a wide range from 10^4 to 10^9 molecules per cm^3.[70,71] To obtain a more complete knowledge of the sulfuric acid effect in the CH_2O hydrolysis reaction, it is necessary to compare the rate of the naked and sulfuric acid-assisted reactions rather than comparing the reaction energy barriers or the rate constants of the individual reactions. The rate ratio, v_{eff}/v_{un}, listed in Table 1 shows that the reaction with the H_2SO_4 catalytic channel is 8 to 16 orders of magnitude faster than the reaction without H_2SO_4. As a result, H_2SO_4 could efficiently make the CH_2O aldol condensation process more feasible than the uncatalyzed channel both energetically and kinetically.

3.2. Structures and thermodynamic analysis

To elucidate the effect of $C_2H_4O_2$ on sulfuric acid nucleation, structures and thermodynamic values of $(H_2SO_4)_m(C_2H_4O_2)_n$ ($0 \leq m, n \leq 3$) clusters were discussed in this section. The cluster formation steps with optimized structures of global Gibbs free energy minima are shown in Fig. 2, and corresponding enthalpies and entropies for $(H_2SO_4)_m(C_2H_4O_2)_n$ ($0 \leq m, n \leq 3$) clusters formation are shown in Table S1 in the (ESI).† Here, $(H_2SO_4)_m(C_2H_4O_2)_n$ are abbreviated as *m*A*n*B and the values in parentheses are the binding Gibbs free energies calculated using the following equation:

$$\Delta G((SA)_m(C_2H_4O_2)_n) = G((SA)_m(C_2H_4O_2)_n) - m \times G_{SA} - n \times G_{C_2H_4O_2} \quad (11)$$

The cluster formation between a SA and a $C_2H_4O_2$ molecule involves the formation of one hydrogen bond as shown in Fig. 2. The reaction Gibbs free energy for forming $(H_2SO_4)(C_2H_4O_2)$ cluster is found to be -1.78 kcal mol^{-1}. This process is more favorable than the formation of the $(H_2SO_4)(CH_2O)$ complex, with a Gibbs free energy change of -1.15 kcal mol^{-1}, as shown in Table 2. However, it is slightly less favorable than the formation of the $(H_2SO_4)(H_2O)$, with a ΔG of -1.94 kcal mol^{-1}, and significantly less favorable than the formation of H_2SO_4 dimer and $(H_2SO_4)(NH_3)$. This result infers that β-hydroxycarbonyl is stronger for stabilizing SA to promote atmospheric particle nucleation than the simple aldehyde, however, the interaction of β-hydroxycarbonyl with SA is still weaker than that of ammonia.

The two subsequent additions of sulfuric acid molecules to the $(H_2SO_4)(C_2H_4O_2)$ complex *via* the formation of SA–SA hydrogen bonded interactions. These processes are found to be more favorable (*i.e.* -6.31 and -4.60 kcal mol^{-1}) compared to the first H_2SO_4 addition, which is due that the addition of a H_2SO_4 molecule leads to a more reduction in the enthalpy though the clustering process is accompanied by an entropy decrease[7] as the formation of hydrogen bonds leads to a more constrained structure. From the molecular structures of these clusters, it is apparent that the interactions strength are as follows: sulfuric acid-sulfuric acid > β-hydroxycarbonyl-sulfuric acid > β-hydroxycarbonyl-β-hydroxycarbonyl.

The $(H_2SO_4)_2(C_2H_4O_2)_2$ cluster formation *via* adding a H_2SO_4 molecule to $(SA)(C_2H_4O_2)_2$ is more favorable than adding a $C_2H_4O_2$ molecule to $(H_2SO_4)_2(C_2H_4O_2)$. However, because the formation of $(H_2SO_4)_2(C_2H_4O_2)$ is more favorable than the formation of $(H_2SO_4)(C_2H_4O_2)_2$, where the corresponding Gibbs free energy changes from $(H_2SO_4)_2(C_2H_4O_2)$ are -6.31 and -2.61 kcal mol^{-1}, respectively, the $(H_2SO_4)_2(C_2H_4O_2)_2$ cluster would be formed along $(H_2SO_4)(C_2H_4O_2) \rightarrow (H_2SO_4)_2(C_2H_4O_2) \rightarrow (H_2SO_4)_2(C_2H_4O_2)_2$ path. The $(H_2SO_4)_3(C_2H_4O_2)_3$ cluster formation shows this feature as well, with the path along $(H_2SO_4)(C_2H_4O_2) \rightarrow (H_2SO_4)_2(C_2H_4O_2) \rightarrow (H_2SO_4)_3(C_2H_4O_2) \rightarrow (H_2SO_4)_3(C_2H_4O_2)_2 \rightarrow (H_2SO_4)_3(C_2H_4O_2)_3$. Looking to the molecular structures of these clusters, the pattern is also due to the different interaction strength levels between molecules. The above pathways are not unique due that the channels are competing with each other and there is an actual channel

Table 2 Enthalpies, entropies, and Gibbs free energies changes associated with the affinities of hydroxyacetaldehyde/formaldehyde to monomers, dimers and trimers of sulfuric acid calculated at the PW91PW91/6-311++G(3df,3pd) level of theory at 298.15 K and 1 atm

Reactions	ΔH (kcal mol^{-1})	ΔS (cal mol^{-1} K^{-1})	ΔG (kcal mol^{-1})
$H_2SO_4 + C_2H_4O_2 \Leftrightarrow (H_2SO_4)(C_2H_4O_2)$	−11.16	−31.47	−1.78
$H_2SO_4 + CH_2O \Leftrightarrow (H_2SO_4)(CH_2O)$	−10.34	−30.82	−1.15
$H_2SO_4 + H_2O \Leftrightarrow (H_2SO_4)(H_2O)$	−11.84	−33.19	−1.94
$H_2SO_4 + NH_3 \Leftrightarrow (H_2SO_4)(NH_3)$	−20.82	−31.96	−11.29
$H_2SO_4 + H_2SO_4 \Leftrightarrow (H_2SO_4)_2$	−16.54	−37.49	−5.36
$(H_2SO_4)_2 + C_2H_4O_2 \Leftrightarrow (H_2SO_4)_2(C_2H_4O_2)$	−13.91	−37.51	−2.72
$(H_2SO_4)_2 + CH_2O \Leftrightarrow (H_2SO_4)_2(CH_2O)$	−10.65	−29.80	−1.77
$(H_2SO_4)_2 + H_2O \Leftrightarrow (H_2SO_4)_2(H_2O)$	−14.28	−36.56	−3.38
$(H_2SO_4)_2 + NH_3 \Leftrightarrow (H_2SO_4)_2(NH_3)$	−29.20	−40.85	−17.02
$(H_2SO_4)_2 + H_2SO_4 \Leftrightarrow (H_2SO_4)_3$	−15.19	−42.02	−2.66
$(H_2SO_4)_3 + C_2H_4O_2 \Leftrightarrow (H_2SO_4)_3(C_2H_4O_2)$	−15.46	−36.17	−4.67
$(H_2SO_4)_3 + CH_2O \Leftrightarrow (H_2SO_4)_3(CH_2O)$	−13.86	−34.39	−3.60
$(H_2SO_4)_3 + H_2O \Leftrightarrow (H_2SO_4)_3(H_2O)$	−17.48	−37.57	−6.28
$(H_2SO_4)_3 + NH_3 \Leftrightarrow (H_2SO_4)_3(NH_3)$	−30.78	−32.88	−20.97
$(H_2SO_4)_3 + H_2SO_4 \Leftrightarrow (H_2SO_4)_4$	−14.73	−42.27	−2.13

occupancy (growth flux) considering the cluster evaporation rate. In the following simulations of steady-state formation rates, growth fluxes were considered.

Comparing the affinity of $C_2H_4O_2$ and CH_2O to dimers and trimers of sulfuric acid as shown in Table 2, similar to the reaction between $C_2H_4O_2$ and H_2SO_4 molecule, the $C_2H_4O_2$ affinity to dimers/trimers of sulfuric acid, with a value of -4.73/-6.67 kcal mol^{-1}, is higher than that the CH_2O affinity, however, it is much less than the corresponding ammonia affinity. In addition, the $C_2H_4O_2$ affinities to sulfuric acid dimer and sulfuric acid trimer are higher than that sulfuric acid itself with a value of -2.66 and -2.13 kcal mol^{-1}, respectively. Here, it once again proves that β-hydroxycarbonyl is stronger for stabilizing sulfuric acid and its polymer to promote nucleation than simple aldehydes. In conclusion, aldol condensation of CH_2O can apparently enhance the binding strength with the atmospheric nucleation precursor of sulfuric acid and its polymer by introducing a functional hydroxyl group. CH_2O and its atmospheric derivatives are unlikely to be key species directly involved in nucleation, such as ammonia and amines. All optimized Cartesian coordinates of $(H_2SO_4)_m(C_2H_4O_2)_n$ ($0 \le m$, $n \le 3$), $(H_2SO_4)_m(H_2O)$ ($0 \le m \le 3$) and $(H_2SO_4)_m(NH_3)$ ($0 \le m \le 3$) discussed here are shown in Table S2 in the ESI.† The optimized structures and Cartesian coordinates for $(H_2SO_4)_m(CH_2O)_n$ ($0 \le m$, $n \le 3$) clusters be found in our previous study.[28]

3.3. Kinetics analysis

3.3.1. Cluster Gibbs free energy surfaces. In order to check whether the nucleation barrier is high or not or maybe nonexistent, the Gibbs free energy change, ΔG, should be converted into the actual Gibbs free energy change,[72]

$$\Delta G_a(P_1, P_2) = \Delta G - k_B T\left[N_1 \ln\left(\frac{P_1}{P_{ref}}\right) + N_2 \ln\left(\frac{P_2}{P_{ref}}\right)\right] \quad (12)$$

where k_B is the Boltzmann constant, T is the temperature, P_{ref} is the reference pressure (1 atm in this case), N_1 and N_2 is the molecule number in the cluster for composition 1 and 2, respectively, and P_1 and P_2 is the partial pressure of component 1 and component 2 in vapor phase, respectively. Here, 1 and 2 means SA and B (CH_2O or $C_2H_4O_2$). Fig. 3 shows the actual formation Gibbs free energy surface (in kcal mol^{-1}) on the SA–B grid at 278.15 K, SA concentration of 10^7 molecules per cm^3, and 1000 pptv of B.

While the absolute value of the formation Gibbs free energies varies between the different systems, a similar trend is seen for the two cases, with a large Gibbs free energy barrier in all directions for forming larger clusters. For any given cluster there is no growth direction that leads to a lower formation Gibbs free energy *via* addition of either B or SA. Following the path with lowest Gibbs free energy from (SA)(B) cluster, the order of growth for the H_2SO_4–$C_2H_4O_2$ systems is continuous addition of a $C_2H_4O_2$ molecule, which is different from the cluster formation steps only considering Gibbs free energy change as shown in Fig. 3, while, the order of growth for the H_2SO_4–CH_2O system is firstly addition of a H_2SO_4 molecule followed by addition of a CH_2O molecule. In general, it is seen that the Gibbs free energy steeply increases towards the system boundaries for these two cases, which implies that the growth within the system is unfavorable.

3.3.2. Evaporation rates. The competition between the forward reaction by adding a molecule and the reverse reaction by evaporation at each intermediate step determines whether a cluster grows to form a nanoparticle, and the collision and evaporation rates can be used to infer the stability of clusters. The total evaporation rates for the $(H_2SO_4)_m(B)_n$ ($0 \le m$, $n \le 3$; "B" represents CH_2O or $C_2H_4O_2$) clusters on the H_2SO_4–B grid at 278.15 K are shown in Fig. 4. While the evaporation rates for clusters vary between the different systems, the evaporation rates for most $(H_2SO_4)_m(C_2H_4O_2)_n$ ($0 \le m$, $n \le 3$) clusters are lower than those for the $(H_2SO_4)_m(CH_2O)_n$ ($0 \le m$, $n \le 3$) clusters. This indicates that $(H_2SO_4)_m(C_2H_4O_2)_n$ ($0 \le m$, $n \le 3$) clusters are more stable than those CH_2O-involved clusters. In H_2SO_4–$C_2H_4O_2$ system, clusters with a higher number of H_2SO_4 than $C_2H_4O_2$ molecules have lower evaporation rates, for example, evaporation rates of $(H_2SO_4)_2(C_2H_4O_2)_1$ and

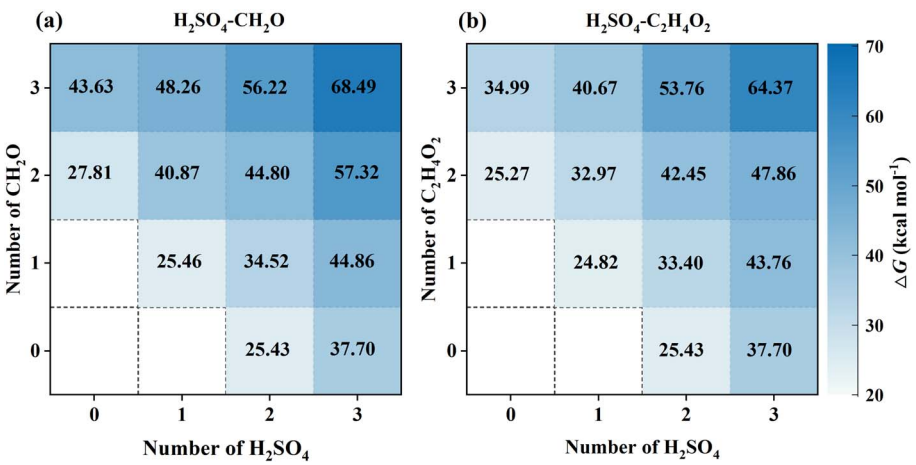

Fig. 3 Gibbs free energy surface of the H_2SO_4–CH_2O system in figure (a) and H_2SO_4–$C_2H_4O_2$ system in figure (b) calculated with PW91PW91/6-311++G(3df,3pd) at 278.15 K, $[H_2SO_4] = 10^7$ molecules per cm^3, and [B] = 1000 pptv.

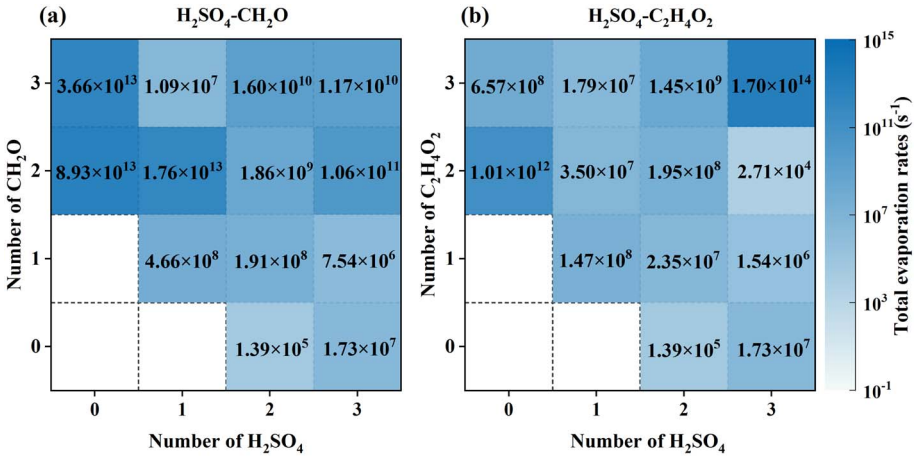

Fig. 4 The total evaporation rates for the $(H_2SO_4)_m(CH_2O)_n$ ($0 \le m, n \le 3$) clusters in figure (a) and $(H_2SO_4)_m(C_2H_4O_2)_n$ ($0 \le m, n \le 3$) clusters in figure (b) at the PW91PW91/6-311++G(3df,3pd) level of theory at 278.15 K.

$(H_2SO_4)_3(C_2H_4O_2)_2$ are smaller than those of $(H_2SO_4)_1(C_2H_4O_2)_2$ and $(H_2SO_4)_2(C_2H_4O_2)_3$, respectively. Therefore, clusters with a higher number of H_2SO_4 than $C_2H_4O_2$ molecules are more stable. In general, the total evaporation rates for the H_2SO_4–$C_2H_4O_2$ and H_2SO_4–CH_2O system are high. Therefore, it is unlikely that B and SA by themselves drive new particle formation at 278 K. In addition, higher concentrations of precursors can enhance the stability of clusters, as higher precursor concentrations increase the probability of cluster collisions and shift the balance between collision and evaporation forward. The effect of the precursors concentrations on the particle formation rate will be discussed next.

3.3.3. Steady-state formation rates. New particles could form when the collision rate of monomers to the clusters exceed the cluster evaporation rates beyond some cluster size. Fig. 5 shows the steady-state formation rate of particles (J) growing out of the simulation systems as a function of monomer concentration at 278.15 K for H_2SO_4–CH_2O and H_2SO_4–$C_2H_4O_2$ systems. The simulations were performed at ambient SA concentrations starting from 10^6 to 10^8 molecules per cm^3 and at ambient CH_2O and $C_2H_4O_2$ concentrations for comparing.

Generally, J increase with increasing the concentrations of B and H_2SO_4 at the simulated condition. The H_2SO_4 concentration dependence of the cluster formation rate does not change with CH_2O and $C_2H_4O_2$ concentration, with the power dependency of 3; the power dependency on $C_2H_4O_2$ does not change with SA concentration, with the value of about 4. J of the H_2SO_4–$C_2H_4O_2$ system are 7–8 orders of magnitude greater than those

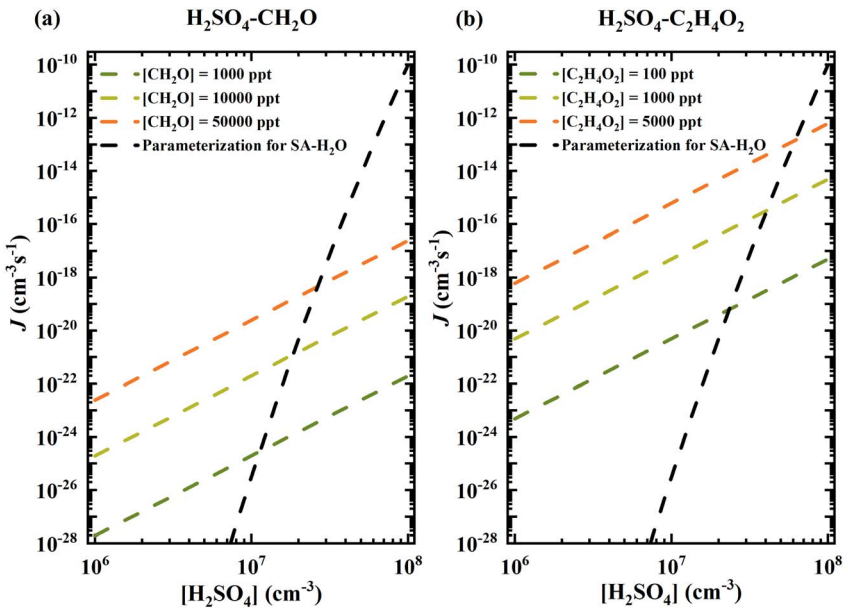

Fig. 5 Simulated particle formation rate J (cm^{-3} s^{-1}) out of the simulation system as a function of H_2SO_4 monomer concentration at 278.15 K with different B mixing ratios for H_2SO_4–CH_2O system in figure (a) and H_2SO_4–$C_2H_4O_2$ system in figure (b). The dashed black lines show the prediction calculated using the parameterized binary homogeneous nucleation of H_2SO_4–H_2O at 278.15 K and RH = 38%.

of the H_2SO_4–CH_2O system at the same conditions with [B] = 1000 ppt. Furthermore, J of the H_2SO_4–$C_2H_4O_2$ system are higher than those of H_2SO_4–H_2O binary homogeneous nucleation at 278.15 K and 38% relative humidity (RH) according to the parameterization suggested by Vehkamäki *et al.*[73] when SA concentration is less than 6×10^7 molecules per cm^3, indicating that the cluster formation for SA with $C_2H_4O_2$ is more favorable than that with water at ambient low SA concentration and low RHs.

4. Conclusions

Aldehydes were speculated as important precursor species in the NPF, and aldol condensation of formaldehyde introduces functional group of –OH and would have lower vapor pressure, hence aldol condensation product is thought to participated in atmospheric NPF. The kinetics of CH_2O aldol condensation to produce $C_2H_4O_2$ was examined and the potential role of $C_2H_4O_2$ in sulfuric acid-driven atmospheric NPF was explored. Structures and thermodynamics up to the cluster size of $(H_2SO_4)_3(B)_3$ are studied, and geometries and ΔG values calculated at 298.15 K and 1 atm show that the $C_2H_4O_2$ likely stabilize sulfuric acid and its polymer better than CH_2O.

This study is based on our previous research on NPF involving hydrolysate of formaldehyde and serves as the first kinetic investigation of clusters containing SA and aldol condensation product of formaldehyde. Particle formation rates for H_2SO_4–$C_2H_4O_2$ system are much higher than those for H_2SO_4–CH_2O system and higher than those of H_2SO_4–H_2O binary homogeneous nucleation at ambient low SA concentration and low RHs. However, the growth of H_2SO_4–$C_2H_4O_2$ clusters is essentially limited by a weak formation of the largest clusters studied. Therefore, the direct involvement of aldol condensation product of formaldehyde in sulfuric acid nucleation is negligible, and other stabilizing vapors are required in sulfuric acid-driven atmospheric NPF. In view of the rich content of carbonyls and different carbonyls show different capabilities to participate in the NPF, the role of higher aldehydes and dicarbonyls in atmospheric particle nucleation and further growth deserve study in the future.

Data availability

The data that support the findings of this study are available on request from the corresponding author, [Chunyu Wang, cyw2022@chu.edu.cn], upon reasonable request.

Author contributions

NT and LZ performed investigation, calculations, visualization, analyzed the data and wrote original draft; CW instructed the design of the algorithm, performed investigation, and revised the manuscript; JC and YP helped to interpret the results and revised the manuscript; HX helped analyzed the data. All authors contributed to the manuscript preparation and approved the submitted version.

Conflicts of interest

There are no conflicts to declare.

Acknowledgements

This work was supported by the National Natural Science Foundation of China (grant no. 42107112), Natural Science Foundation of Anhui Province (grant no. 2308085QD130), Provincial Undergraduate Training Program for Innovation and Entrepreneurship (S202310380105), Key Scientific Research Project of Anhui Education Department (2022AH051712) and Chaohu University for the Start-Up grant (KYQD-202215).

References

1 J. Almeida, S. Schobesberger, A. Kürten, I. K. Ortega, O. Kupiainen-Määttä, A. P. Praplan, A. Adamov, A. Amorim, F. Bianchi, M. Breitenlechner, A. David, J. Dommen, N. M. Donahue, A. Downard, E. Dunne, J. Duplissy, S. Ehrhart, R. C. Flagan, A. Franchin, R. Guida, J. Hakala, A. Hansel, M. Heinritzi, H. Henschel, T. Jokinen, H. Junninen, M. Kajos, J. Kangasluoma, H. Keskinen, A. Kupc, T. Kurtén, A. N. Kvashin, A. Laaksonen, K. Lehtipalo, M. Leiminger, J. Leppä, V. Loukonen, V. Makhmutov, S. Mathot, M. J. McGrath, T. Nieminen, T. Olenius, A. Onnela, T. Petäjä, F. Riccobono, I. Riipinen, M. Rissanen, L. Rondo, T. Ruuskanen, F. D. Santos, N. Sarnela, S. Schallhart, R. Schnitzhofer, J. H. Seinfeld, M. Simon, M. Sipilä, Y. Stozhkov, F. Stratmann, A. Tomé, J. Tröstl, G. Tsagkogeorgas, P. Vaattovaara, Y. Viisanen, A. Virtanen, A. Vrtala, P. E. Wagner, E. Weingartner, H. Wex, C. Williamson, D. Wimmer, P. Ye, T. Yli-Juuti, K. S. Carslaw, M. Kulmala, J. Curtius, U. Baltensperger, D. R. Worsnop, H. Vehkamäki and J. Kirkby, *Nature*, 2013, **502**, 359.

2 M. Ehn, J. A. Thornton, E. Kleist, M. Sipila, H. Junninen, I. Pullinen, M. Springer, F. Rubach, R. Tillmann, B. Lee, F. Lopez-Hilfiker, S. Andres, I. H. Acir, M. Rissanen, T. Jokinen, S. Schobesberger, J. Kangasluoma, J. Kontkanen, T. Nieminen, T. Kurten, L. B. Nielsen, S. Jorgensen, H. G. Kjaergaard, M. Canagaratna, M. D. Maso, T. Berndt, T. Petaja, A. Wahner, V. M. Kerminen, M. Kulmala, D. R. Worsnop, J. Wildt and T. F. Mentel, *Nature*, 2014, **506**, 476–479.

3 M. Kulmala, I. Riipinen, M. Sipilä, H. E. Manninen, T. Petäjä, H. Junninen, M. D. Maso, G. Mordas, A. Mirme, M. Vana, A. Hirsikko, L. Laakso, R. M. Harrison, I. Hanson, C. Leung, K. E. J. Lehtinen and V.-M. Kerminen, *Science*, 2007, **318**, 89.

4 F. Bianchi, J. Tröstl, H. Junninen, C. Frege, S. Henne, C. R. Hoyle, U. Molteni, E. Herrmann, A. Adamov, N. Bukowiecki, X. Chen, J. Duplissy, M. Gysel, M. Hutterli, J. Kangasluoma, J. Kontkanen, A. Kürten, H. E. Manninen, S. Münch, O. Peräkylä, T. Petäjä, L. Rondo, C. Williamson, E. Weingartner, J. Curtius, D. R. Worsnop, M. Kulmala,

J. Dommen and U. Baltensperger, *Science*, 2016, **352**, 1109–1112.

5 M. Sipilä, T. Berndt, T. Petäjä, D. Brus, J. Vanhanen, F. Stratmann, J. Patokoski, R. L. Mauldin, A.-P. Hyvärinen, H. Lihavainen and M. Kulmala, *Science*, 2010, **327**, 1243–1246.

6 J. Kirkby, J. Curtius, J. o. Almeida, E. Dunne, J. Duplissy, S. Ehrhart, A. Franchin, S. P. Gagné, L. Ickes, A. Kürten, A. Kupc, A. Metzger, F. Riccobono, L. Rondo, S. Schobesberger, G. Tsagkogeorgas, D. Wimmer, A. Amorim, F. Bianchi, M. Breitenlechner, A. David, J. Dommen, A. Downard, M. Ehn, R. C. Flagan, S. Haider, A. Hansel, D. Hauser, W. Jud, H. Junninen, F. Kreissl, A. Kvashin, A. Laaksonen, K. Lehtipalo, J. Lima, E. R. Lovejoy, V. Makhmutov, S. Mathot, J. Mikkilä, P. Minginette, S. Mogo, T. Nieminen, A. Onnela, P. Pereira, T. Petäjä, R. Schnitzhofer, J. H. Seinfeld, M. Sipilä, Y. Stozhkov, F. Stratmann, A. Tomé, J. Vanhanen, Y. Viisanen, A. Vrtala, P. E. Wagner, H. Walther, E. Weingartner, H. Wex, P. M. Winkler, K. S. Carslaw, D. R. Worsnop, U. Baltensperger and M. Kulmala, *Nature*, 2011, **476**, 429–433.

7 R. Zhang, A. Khalizov, L. Wang, M. Hu and W. Xu, *Chem. Rev.*, 2012, **112**, 1957–2011.

8 J. Tröstl, W. K. Chuang, H. Gordon, M. Heinritzi, C. Yan, U. Molteni, L. Ahlm, C. Frege, F. Bianchi, R. Wagner, M. Simon, K. Lehtipalo, C. Williamson, J. S. Craven, J. Duplissy, A. Adamov, J. Almeida, A.-K. Bernhammer, M. Breitenlechner, S. Brilke, A. Dias, S. Ehrhart, R. C. Flagan, A. Franchin, C. Fuchs, R. Guida, M. Gysel, A. Hansel, C. R. Hoyle, T. Jokinen, H. Junninen, J. Kangasluoma, H. Keskinen, J. Kim, M. Krapf, A. Kürten, A. Laaksonen, M. Lawler, M. Leiminger, S. Mathot, O. Möhler, T. Nieminen, A. Onnela, T. Petäjä, F. M. Piel, P. Miettinen, M. P. Rissanen, L. Rondo, N. Sarnela, S. Schobesberger, K. Sengupta, M. Sipilä, J. N. Smith, G. Steiner, A. Tomè, A. Virtanen, A. C. Wagner, E. Weingartner, D. Wimmer, P. M. Winkler, P. Ye, K. S. Carslaw, J. Curtius, J. Dommen, J. Kirkby, M. Kulmala, I. Riipinen, D. R. Worsnop, N. M. Donahue and U. Baltensperger, *Nature*, 2016, **533**, 527–531.

9 Y. Xu, A. B. Nadykto, F. Yu, L. Jiang and W. Wang, *J. Mol. Struct.:THEOCHEM*, 2010, **951**, 28–33.

10 A. Metzger, B. Verheggen, J. Dommen, J. Duplissy, A. S. Prevot, E. Weingartner, I. Riipinen, M. Kulmala, D. V. Spracklen, K. S. Carslaw and U. Baltensperger, *Proc. Natl. Acad. Sci. U. S. A.*, 2010, **107**, 6646–6651.

11 C. Kuang, M. Chen, J. Zhao, J. Smith, P. H. McMurry and J. Wang, *Atmos. Chem. Phys.*, 2012, **12**, 3573–3589.

12 L. Liu, F. Yu, L. Du, Z. Yang, J. S. Francisco and X. Zhang, *Proc. Natl. Acad. Sci. U. S. A.*, 2021, **118**, e2108384118.

13 R. Zhang, I. Suh, J. Zhao, D. Zhang, E. C. Fortner, X. Tie, L. T. Molina and M. J. Molina, *Science*, 2004, **304**, 1487–1490.

14 R. McGraw and R. Zhang, *J. Chem. Phys.*, 2008, **128**, 064508.

15 D. Schwela, *Encyclopedia of Toxicology*, Acad. Press Oxf, 2014, pp. 1003–1017.

16 W. Xiaoyan, W. Huixiang and W. Shaoli, *Atmos. Environ.*, 2010, **44**, 2074–2078.

17 M. Possanzini, V. D. Palo and A. Cecinato, *Atmos. Environ.*, 2002, **36**, 3195–3201.

18 J. Zheng, R. Zhang, J. P. Garzón, M. E. Huertas, M. Levy, Y. Ma, R. Torres-Jardón, L. G. Ruiz-Suárez, L. Russell, S. Takahama, H. Tan, G. Li and L. T. Molina, *Atmos. Environ.*, 2013, **70**, 513–520.

19 D. J. Jacob, *Atmos. Environ.*, 2000, **34**, 2131–2159.

20 V. Wagner, R. von Glasow, H. Fischer and P. J. Crutzen, *J. Geophys. Res.:Atmos.*, 2002, **107**, 4341.

21 G. Li, H. Su, X. Li, U. Kuhn, H. Meusel, T. Hoffmann, M. Ammann, U. Pöschl, M. Shao and Y. Cheng, *Atmos. Chem. Phys.*, 2016, **16**, 10299–10311.

22 X. Zhou, Y.-N. Lee, L. Newman, X. Chen and K. Mopper, *J. Geophys. Res.:Atmos.*, 1996, **101**, 14711–14719.

23 X. Tie, G. Brasseur, L. Emmons, L. Horowitz and D. Kinnison, *J. Geophys. Res.:Atmos.*, 2001, **106**, 22931–22964.

24 A. Fried, J. Crawford, J. Olson, J. Walega, W. Potter, B. Wert, C. Jordan, B. Anderson, R. Shetter, B. Lefer, D. Blake, N. Blake, S. Meinardi, B. Heikes, D. O'Sullivan, J. Snow, H. Fuelberg, C. M. Kiley, S. Sandholm, D. Tan, G. Sachse, H. Singh, I. Faloona, C. N. Harward and G. R. Carmichael, *J. Geophys. Res.:Atmos.*, 2003, **108**, 8798.

25 X. Shi, R. Zhang, Y. Sun, F. Xu, Q. Zhang and W. Wang, *Phys. Chem. Chem. Phys.*, 2018, **20**, 1005–1011.

26 C.-Y. Wang, S. Jiang, Z.-Q. Wang, Y.-R. Liu, H. Wen, T. Huang, Y.-J. Han and W. Huang, *Atmos. Environ.*, 2019, **201**, 323–333.

27 G. Zhang, M. Liu, Y. Han, Z. Wang, W. Liu, Y. Zhang and J. Xu, *RSC Adv.*, 2024, **14**, 13321–13335.

28 C. Wang, X. Chen, Y. Liu, T. Huang and S. Jiang, *ACS Omega*, 2023, **8**, 15467–15478.

29 K. C. Barsanti and J. F. Pankow, *Atmos. Environ.*, 2004, **38**, 4371–4382.

30 M. Jang and R. M. Kamens, *Environ. Sci. Technol.*, 2001, **35**, 4758–4766.

31 L. N. Hawkins, M. J. Baril, N. Sedehi, M. M. Galloway, D. O. De Haan, G. P. Schill and M. A. Tolbert, *Environ. Sci. Technol.*, 2014, **48**, 2273–2280.

32 A. Lee, H. Goldstein Allen, H. Kroll Jesse, L. Ng Nga, V. Varutbangkul, C. Flagan Richard and H. Seinfeld John, *J. Geophys. Res.:Atmos.*, 2006, **111**, D17305.

33 S. Spaulding Reggie, W. Schade Gunnar, H. Goldstein Allen and M. J. Charles, *J. Geophys. Res.:Atmos.*, 2003, **108**, 4247.

34 H. Niki, P. D. Maker, C. M. Savage and L. P. Breitenbach, *Chem. Phys. Lett.*, 1981, **80**, 499–503.

35 I. Bertschi, J. Yokelson Robert, E. Ward Darold, E. Babbitt Ron, A. Susott Ronald, G. Goode Jon and M. Hao Wei, *J. Geophys. Res.:Atmos.*, 2003, **108**, 8472.

36 X. H. Zhou, G. Civerolo and K. Schwab, *Environ. Sci. Technol.*, 2009, **43**, 2753–2759.

37 Y.-N. Lee, X. Zhou, L. I. Kleinman, L. J. Nunnermacker, S. R. Springston, P. H. Daum, L. Newman, W. G. Keigley, M. W. Holdren, C. W. Spicer, V. Young, B. Fu, D. D. Parrish, J. Holloway, J. Williams, J. M. Roberts,

T. B. Ryerson and F. C. Fehsenfeld, *J. Geophys. Res.:Atmos.*, 1998, **103**, 22449–22462.
38 M. J. Perri, S. Seitzinger and B. J. Turpin, *Atmos. Environ.*, 2009, **43**, 1487–1497.
39 K. Shashikala, P. M. Niha, J. Aswathi, J. Sharanya and D. Janardanan, *Comput. Theor. Chem.*, 2023, **1222**, 114057.
40 M. J. McGrath, T. Olenius, I. K. Ortega, V. Loukonen, P. Paasonen, T. Kurtén, M. Kulmala and H. Vehkamäki, *Atmos. Chem. Phys.*, 2012, **12**, 2345–2355.
41 T. Olenius, O. Kupiainen-Määttä, I. K. Ortega, T. Kurtén and H. Vehkamäki, *J. Chem. Phys.*, 2013, **139**, 084312.
42 J.-W. Yoon, J.-H. Park, C.-C. Shur and S.-B. Jung, *Microelectron. Eng.*, 2007, **84**, 2552–2557.
43 D. J. Wales and J. P. K. Doye, *J. Phys. Chem. A*, 1997, **101**, 5111–5116.
44 W. Huang, R. Pal, L.-M. Wang, X. C. Zeng and L.-S. Wang, *J. Chem. Phys.*, 2010, **132**, 054305.
45 J. J. Stewart, *J. Mol. Model.*, 2013, **19**, 1–32.
46 W. Huang, M. Ji, C.-D. Dong, X. Gu, L.-M. Wang, X. G. Gong and L.-S. Wang, *ACS Nano*, 2008, **2**, 897–904.
47 W. Huang, A. P. Sergeeva, H.-J. Zhai, B. B. Averkiev, L.-S. Wang and A. I. Boldyrev, *Nat. Chem.*, 2010, **2**, 202–206.
48 C. Wang, Y. Liu, T. Huang, Y. Feng, Z. Wang, R. Lu and S. Jiang, *Phys. Chem. Chem. Phys.*, 2022, **24**, 23540–23550.
49 M. J. Frisch, H. B. Schlegel, G. E. Scuseria, M. A. Robb, G. Scalmani, V. Barone, B. Mennucci, G. A. Petersson, M. Caricato, X. Li, H. P. Hratchian, A. F. Izmaylov, G. Zheng, J. L. Sonnenberg and M. Hada, *Gaussian*, Gaussian Inc., Wallingford CT, 2009.
50 T. Kurtén, L. Torpo, C.-G. Ding, H. Vehkamäki, M. R. Sundberg, K. Laasonen and M. Kulmala, *J. Geophys. Res.:Atmos.*, 2007, **112**, D04210.
51 A. B. Nadykto, F. Yu and J. Herb, *Phys. Chem. Chem. Phys.*, 2008, **10**, 7073–7078.
52 A. B. Nadykto, H. Du and F. Yu, *Vib. Spectrosc.*, 2007, **44**, 286–296.
53 A. B. Nadykto and F. Yu, *Chem. Phys. Lett.*, 2007, **435**, 14–18.
54 C.-Y. Wang, S. Jiang, Y.-R. Liu, H. Wen, Z.-Q. Wang, Y.-J. Han, T. Huang and W. Huang, *J. Phys. Chem. A*, 2018, **122**, 3470–3479.
55 H. Wen, T. Huang, C.-Y. Wang, X.-Q. Peng, S. Jiang, Y.-R. Liu and W. Huang, *Atmos. Environ.*, 2018, **191**, 214–226.
56 Y. Zhao and D. G. Truhlar, *Theor. Chem. Acc.*, 2008, **120**, 215–241.
57 M. J. Frisch, J. A. Pople and J. S. Binkley, *J. Chem. Phys.*, 1984, **80**, 3265–3269.
58 K. Fukui, *Acc. Chem. Res.*, 1981, **14**, 471–476.
59 F. Neese, *Wiley Interdiscip. Rev. Comput. Mol. Sci.*, 2018, **8**, e1327.
60 C. Eckart, *Phys. Rev.*, 1930, **35**, 1303–1309.
61 D. G. Truhlar, B. C. Garrett and S. J. Klippenstein, *J. Phys. Chem.*, 1996, **100**, 12771–12800.
62 S. Canneaux, F. Bohr and E. Henon, *J. Comput. Chem.*, 2014, **35**, 82–93.
63 H. Henschel, T. Kurten and H. Vehkamaki, *J. Phys. Chem. A*, 2016, **120**, 1886–1896.
64 O. Kupiainen, I. Ortega, T. Kurtén and H. Vehkamäki, *Atmos. Chem. Phys.*, 2012, **12**, 3591–3599.
65 B. Long, X.-F. Tan, C.-R. Chang, W.-X. Zhao, Z.-W. Long, D.-S. Ren and W.-J. Zhang, *J. Phys. Chem. A*, 2013, **117**, 5106–5116.
66 V. Hirvonen, N. Myllys, T. Kurten and J. Elm, *J. Phys. Chem. A*, 2018, **122**, 1771–1780.
67 L. Liu, J. Zhong, H. Vehkamäki, T. Kurtén, L. Du, X. Zhang, J. S. Francisco and X. C. Zeng, *Proc. Natl. Acad. Sci. U. S. A.*, 2019, **116**, 24966–24971.
68 H. Fliegl, A. Glöß, O. Welz, M. Olzmann and W. Klopper, *J. Chem. Phys.*, 2006, **125**, 054312.
69 G.-B. Li, S.-H. Cai and B. Long, *ACS Omega*, 2022, **7**, 39671–39679.
70 F. Bianchi, J. Tröstl, H. Junninen, C. Frege, S. Henne, C. R. Hoyle, U. Molteni, E. Herrmann, A. Adamov, N. Bukowiecki, X. Chen, J. Duplissy, M. Gysel, M. Hutterli, J. Kangasluoma, J. Kontkanen, A. Kürten, H. E. Manninen, S. Münch, O. Peräkylä, T. Petäjä, L. Rondo, C. Williamson, E. Weingartner, J. Curtius, D. R. Worsnop, M. Kulmala, J. Dommen and U. Baltensperger, *Science*, 2016, **352**, 1109–1112.
71 L. Yang, W. Nie, Y. Liu, Z. Xu, M. Xiao, X. Qi, Y. Li, R. Wang, J. Zou, P. Paasonen, C. Yan, Z. Xu, J. Wang, C. Zhou, J. Yuan, J. Sun, X. Chi, V.-M. Kerminen, M. Kulmala and A. Ding, *Environ. Sci. Technol.*, 2021, **55**, 6665–6676.
72 H. Vehkamäki, *Classical Nucleation Theory in Multicomponent Systems*, Springer, Berlin/Heidelberg, Germany, 2006.
73 H. Vehkamäki, M. Kulmala, I. Napari, K. E. J. Lehtinen, C. Timmreck, M. Noppel and A. Laaksonen, *J. Geophys. Res.:Atmos.*, 2002, **107**, 4622.